JOURNAL OF AGRICULTURAL AND FOOD CHEMISTRY

pubs.acs.org/JAFC

Article

Preparation of Boronic Acid-Functionalized Cryogels Using Modular and Clickable Building Blocks for Bacterial Separation

Hongwei Zheng, Solmaz Hajizadeh, Haiyue Gong, Hong Lin, and Lei Ye*

Cite This: *J. Agric. Food Chem.* 2021, 69, 135−145

Read Online

ACCESS | Metrics & More | Article Recommendations | Supporting Information

ABSTRACT: Composite cryogels containing boronic acid ligands are synthesized for effective separation and isolation of bacteria. The large and interconnected pores in cryogels enable fast binding and release of microbial cells. To control bacterial binding, an alkyne-tagged boronic acid ligand is conjugated to azide-functionalized cryogel *via* the Cu(I)-catalyzed azide−alkyne cycloaddition reaction. The boronic acid-functionalized cryogel binds Gram-positive and Gram-negative bacteria through reversible boronate ester bonds, which can be controlled by pH and simple monosaccharides. To increase the capacity of affinity separation, a new approach is used to couple the alkyne-tagged phenylboronic acid to cryogel *via* an intermediate polymer layer that provides multiple immobilization sites. The morphology and chemical composition of the composite cryogel are characterized systematically. The capability of the composite cryogel for the separation of Gram-positive and Gram-negative bacteria is investigated. The binding capacities of the composite cryogel for *Escherichia coli* and *Staphylococcus epidermidis* are 2.15×10^9 and 3.36×10^9 cfu/g, respectively. The bacterial binding of the composite cryogel can be controlled by adjusting pH. The results suggest that the composite cryogel may be used as affinity medium for rapid separation and isolation of bacteria from complex samples.

KEYWORDS: *composite cryogel, reversible addition fragmentation chain transfer polymerization, boronate affinity, bacteria, bioseparation*

INTRODUCTION

Rapid detection of bacteria is essential for diminishing outbreaks of pathogenic bacteria in living environments, clinical and hospital buildings, and food production plants.[1−3] To reduce the risk of bacterial contamination, novel detection techniques based on immunological, genetic, and spectroscopic signature of bacteria are being developed.[4,5] The new analytical methods are rapid and sensitive, with a capability to detect even a single cell in some cases. However, these methods have not been fully exploited in practical applications because of the difficulty of separating target bacteria from interfering substances in biological samples.[4−6] Selective isolation and separation of target bacteria is an important step to achieve accurate detection of bacteria. The most commonly used separation methods such as centrifugation, filtration, and affinity chromatography suffer from different limitations including low selectivity, limited sample throughput, and high cost.[7,8]

Currently, boronate affinity materials in the form of monolith,[9,10] nanoparticles,[11−13] hydrogels,[14] cryogel,[15] and multifunctional sensors[16,17] have shown great potential for selective recognition, immobilization, and separation of *cis*-diol-containing molecules and biological assemblies. The pH-sensitive, reversible covalent bond between boronic acids and *cis*-diol-containing molecules in an aqueous solution makes boronic acids ideal ligands for specific recognition of *cis*-diols.[18−20] The presence of poly- and oligosaccharides on the cell surface makes it possible to use a reversible boronate ester bond to separate bacteria.[21,22] Several chemical sensors have been constructed using boronate affinity to capture bacteria.[22−24] To enhance the binding strength of boronic acid, efforts have been made to explore the synergy effect of multiple boronate ester bonds to capture biomacromolecules.[11,19] Dendrimers such as poly(amidoamine) and branched polyethyleneimine have been modified with boronic acids to increase the binding strength to bacteria and glycomolecules.[21,25−27] Linear polymers containing multiple boronic acid groups have also been studied. As a flexible polymer backbone allows the pendant affinity ligands to maximize molecular interactions with targeted glycomolecules and cells, boronic acid-functionalized linear polymers have been attached to different supporting materials to simplify affinity separation and purification.[28−30]

Cryogel is a macroporous material composed of a cross-linked hydrophilic polymer network with well-controlled macroporosity (with pore size between 1 and 100 μm).[31−33] The large pores and interconnected channels of cryogels are the products of cryogelation polymerization.[32] These macroporous structures allow a high flow rate and fast mass transfer, making it possible to realize the direct separation of cells even from complex biological samples without complicated pretreatment processes.[32−36] In contrast to small molecules, bacterial cells cannot enter the inner polymer network of cryogels because of their large physical size. Consequently, affinity ligands for bacterial separation must be immobilized on the

Received: September 22, 2020
Revised: December 12, 2020
Accepted: December 16, 2020
Published: December 29, 2020

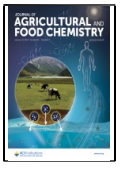

Scheme 1. Preparation of Boronic Acid-Functionalized Cryogels

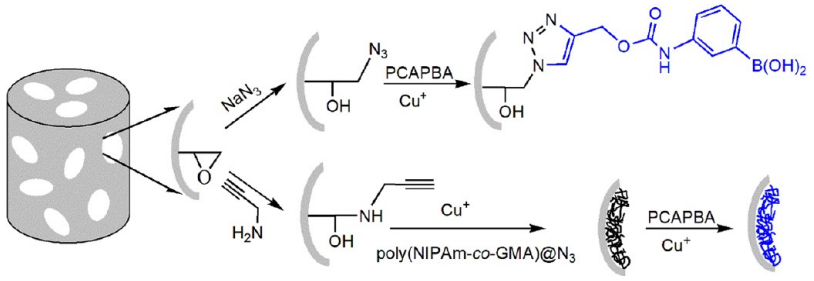

surface of the macropores in cryogel to maximize the efficiency of separation. Still, one major challenge related to using cryogel is the material's low capacity. In previous studies, different types of nanoparticles have been added to cryogels to improve the capacity for the separation of small molecules,[37] proteins, and microbial cells.[34,38]

In this work, we introduce the use of the high-efficiency Cu(I)-catalyzed azide−alkyne cycloaddition (CuAAC) click reaction to immobilize boronic acid on macroporous cryogels for bacterial separation (Scheme 1). To improve the capacity of the affinity material, a flexible polymer chain is also added to increase the number of immobilized boronic acid. A thermoresponsive polymer containing pendant azide groups was synthesized from *N*-isopropylacrylamide and glycidyl methacrylate, using reversible addition−fragmentation chain-transfer (RAFT) polymerization followed by the conversion of the pendant epoxides into azide groups. After the intermediate polymer was conjugated to alkyne-functionalized cryogel using CuAAC, the remaining azide groups on the polymer was used to immobilize the boronic acid ligand through a subsequent CuAAC. Owing to the potency of boronic acid−*cis*-diol bonding and the macroporous structure of cryogel, a novel monolithic column for bioseparation of bacteria was obtained. The physical and chemical properties of the composite cryogel were characterized by Fourier transform infrared (FTIR) spectroscopy and scanning electron microscopy (SEM). Bacterial-binding characteristics of the composite cryogel were studied to reveal the importance of the flexible polymer and the immobilized boronic acid. The feasibility of using the composite cryogel to capture bacteria in the complex sample (25% milk) was also investigated.

EXPERIMENTAL SECTION

Materials. *N*-Isopropylacrylamide (NIPAm), cumyl dithiobenzoate (CDB), glycidyl methacrylate (GMA), 3-aminophenylboronic acid (APBA) hemisulfate salt (≥95%), propargyl chloroformate, acrylamide (Am), *N*,*N*,*N*′,*N*′-tetramethylethylenediamine (TEMED), ammonium persulfate (APS), *N*,*N*′-methylenebis(acrylamide) (MBAm), *N*,*N*-dimethylformamide (DMF), 2-aminoethanol, dimethyl sulfoxide-d_6 (DMSO-d_6), isoamyl acetate, propargylamine, sodium azide, copper(II) sulfate, magnesium sulfate, sodium ascorbate, fructose, acetic acid, and methanol were obtained from Sigma-Aldrich (Steinheim, Germany). Allyl glycidyl ether (AGE) was purchased from EGA-Chemie (Steinheim, Germany). 2,2′-Azobis(2-methylpropionitrile) (AIBN, 98%), ethyl acetate, yeast extract granulated, and agar were obtained from Merck (Darmstadt, Germany). AIBN was recrystallized from methanol before use. Ethanol was purchased from SOLVECO (Rosersberg, Sweden). Tryptone was purchased from Duchefa Biochemie (Haarlem, Netherlands). Sodium hydrogen carbonate, sodium hydroxide, potassium chloride, sodium chloride, di-sodium hydrogen phosphate, potassium dihydrogen phosphate, and ammonium chloride were purchased from Fisher Scientific (Schwerte, Germany). Ultrapure water (18.0 MΩ cm) was procured from an ELGA LabWater System (Vivendi Water Systems Ltd., UK). Milk was purchased from a local market in Lund and was stored at 4 °C before use.

Alkyne-tagged boronic acid, 3-(prop-2-ynyloxycarbonylamino)-phenylboronic acid (PCAPBA), was synthesized according to a previous publication.[39]

Synthesis of Poly(NIPAm-*co*-GMA)@N_3. The thermoresponsive copolymer, poly(NIPAm-*co*-GMA), was synthesized by RAFT polymerization. NIPAm (1.487 g, 13.1 mmol), GMA (570 mg, 4.01 mmol), AIBN (6.2 mg, 0.037 mmol), and CDB (32.6 mg, 0.12 mmol) were dissolved in 25 mL of methanol and charged into a 50 mL flask equipped with a magnetic stirrer. The mixture was cooled using an ice-water bath and nitrogen-purged for 15 min. The flask was sealed and kept at 70 °C under a nitrogen atmosphere for polymerization for 24 h with vigorous stirring. The reaction was terminated by exposing to air, and the product was transferred into a dialysis tube (MWCO 1000 Da) and kept in water for 3 days (with water being replaced for 5−6 times per day). Finally, the polymer was dried using rotary evaporation at 40 °C.

Poly(NIPAm-*co*-GMA) (80 mg), NaN_3 (78 mg), ammonium chloride (64.5 mg), and DMF (7.5 mL) were charged into a glass vial and sealed. The mixture was stirred at 60 °C for 24 h. After the reaction, the polymer was dialyzed in water for 3 days (with the water being replaced for 5−6 times per day) and dried using rotary evaporation at 40 °C.

Synthesis of Epoxy-Functionalized Cryogel (AG). Epoxy-functionalized cryogel was synthesized following a previously established method with slight modifications.[34,38] Briefly, Am (210 mg, 2.0 mmol), MBAm (56 mg, 0.25 mmol), and AGE (35 μL, 0.020 mmol) were dissolved in 4.5 mL of water. After the addition of 7.5 μL (~6 mg) of TEMED, the mixture was cooled on an ice bath and deoxygenated under reduced pressure for 15 min. Subsequently, 6 mg of the initiator APS dissolved in 0.5 mL of water was introduced into the mixture. Aliquots of the mixture (0.5 mL) were immediately transferred into precooled glass tubes (I.D. 7 mm). The polymerization was conducted at −12 °C overnight. After the reaction, the samples were thawed at ambient temperature, washed thoroughly with water to remove residual substances, and then dried in an oven at 60 °C. The obtained cryogel was named AG.

Preparation of Azide-Functionalized Cryogel (AG-N_3). AG cryogel (4 pieces, ~100 mg), NaN_3 (156 mg), ammonium chloride (129 mg), and DMF (15 mL) were added into a 30 mL glass bottle. After sonication for 10 min, the mixture was shaken at 150 rpm in an incubator at 45 °C for 24 h. After the reaction, the cryogel was washed thoroughly with water and dried under reduced pressure. The product was named AG-N_3.

Preparation of Alkyne-Functionalized Cryogel (AG-alkyne). AG cryogel (4 pieces, ~100 mg) was submerged in a solution of propargylamine (2%, v/v) and 2-aminoethanol (4%, v/v) in carbonate buffer (5 mL, 0.1 M, pH 9) and allowed to react at ambient temperature for 24 h. After the reaction, the product was washed consecutively with 100 mL of carbonate buffer and 30 mL of water and then vacuum-dried. The obtained cryogel was named AG-alkyne.

Introduction of Poly(NIPAm-*co*-GMA)@N_3 *via* Click Reaction to Alkyne-Functionalized Cryogel (AG-alkyne@polymer-N_3). Poly(NIPAm-*co*-GMA)@N_3 (120 mg) was dissolved in 10 mL of

https://dx.doi.org/10.1021/acs.jafc.0c06052
J. Agric. Food Chem. 2021, 69, 135−145

methanol:water (4:1, v/v) solution. To the mixture, AG-alkyne (2 pieces, ~50 mg) was added, followed by the addition of 80 μL of 100 mM $CuSO_4$ solution and 8 mg of sodium ascorbate. The mixture was deoxygenated with nitrogen for 15 min and then shaken at 50 °C for 24 h. After the reaction, the cryogel was washed with 30 mL of methanol−water (4:1; v/v) solution and 20 mL water and finally vacuum-dried. The composite cryogel was named AG-alkyne@polymer-N_3.

Introduction of Boronic Acid Ligands *via* Click Reaction on Composite Cryogel. AG-alkyne@polymer-N_3 (2 pieces, ~60 mg) was immersed in a solution of PCAPBA (108 mg) in methanol−water solution (12 mL, 1:1, v/v). After deoxygenation with nitrogen gas for 15 min, 40 μL of 100 mM $CuSO_4$ solution and 4 mg of sodium ascorbate were added into the mixture. The mixture was degassed with nitrogen for another 15 min and then placed on a rocking table at ambient temperature for 24 h. After the reaction, the product was washed thoroughly with 50% methanol−water solution and vacuum-dried. The obtained cryogel was named AG-alkyne@polymer-pBA.

To introduce the PCAPBA on AG-N_3, the same reaction processes were used, and the obtained product was named AG-BA.

Bacterial Cultivation. *Escherichia coli* (*E. coli*) TG1 PTA-4741 and *Staphylococcus epidermidis* (*S. epidermidis*) ATCC12228 strains were obtained from the American Type Culture Collection (ATCC, Manassas, USA). The bacterial strains were grown overnight in 10 mL of Luria−Bertani (LB) medium at 37 °C for 12 h with shaking at 180 rpm. The bacterial cells were isolated by centrifugation at 5000 rpm (3438*g*) for 5 min, washed five times with phosphate-buffered saline (PBS, 0.01 M, pH 7.4), and finally resuspended in 1 mL of PBS. Before binding experiments, the bacterial suspensions were diluted with PBS to give a specified optical density at 600 nm (OD_{600}). The quantification of bacteria was based on a calibration plot between the concentrations of bacteria and the OD_{600} values.

Evaluation of AG-Alkyne@Polymer-pBA for Bacterial Separation. To evaluate the bacterial-binding characteristics of the composite cryogels, the following experiment was conducted. In brief, a cryogel was inserted into a glass tube (I.D. 7 mm). This cryogel column was activated by loading with 10 mL of PBS (0.01 M) with pH adjusted to 6.5 and 8.0, respectively. After this step, 4 mL of *E. coli* or *S. epidermidis* suspension (OD_{600} = 1.9) in the corresponding PBS was circulated through the column at a flow rate of 1 mL/min for 60 min using a peristaltic pump. After every 20 min, the flow direction was reversed to avoid clogging. After the binding, 10 mL of PBS was used to wash out the nonspecifically bound bacteria. The unbound bacteria after the adsorption and the washing were collected and measured at 600 nm to determine the remaining bacteria in the cryogel.

The binding capacity (Q, cfu/g) of the composite cryogel was calculated using the equation

$$Q = \frac{(C_0 - C_1)V_0 - C_2V_1}{m}10^3 \quad (1)$$

where C_0 (cfu/mL) is the initial concentration of bacteria, C_1 (cfu/mL) is the concentration of the unbound bacteria after the adsorption, C_2 (cfu/mL) is the concentration of bacteria in the washing solution, V_0 (mL) is the volume of the bacterial suspension, V_1 (mL) is the volume of the washing solution, and m (mg) is the mass of the composite cryogel.

To investigate the influence of the elution conditions on the recoveries, the bacteria were suspended in PBS (0.01 M, pH 8.0) and adsorbed by the composite cryogel. After washing, the bacteria bound on the composite cryogel was eluted using four different conditions: 3 mL of 0.2 M acetic acid buffer (pH 4.0, containing 0.5 M NaCl), 3 mL of 0.1 M fructose in PBS (20 mM, pH 9.0, containing 0.5 M NaCl), 3 mL of 0.2 M fructose in PBS (20 mM, pH 9.0, containing 0.5 M NaCl), and 3 mL of 0.5 M fructose in PBS (20 mM, pH 9.0, containing 0.5 M NaCl). After loading the eluting buffer, the column outlet was closed, and the bacterial cells were allowed to desorb for 15 min. After this step, the eluting solution was collected by squeezing the cryogel. The concentration of bacteria was measured by spectrophotometric analysis.

Validation with Complex Samples. Aliquots of 4 mL of 25% cow milk (v/v) were incubated with 10^3 cfu/mL of *E. coli* or *S. epidermidis*, separately. After adjusting the sample pH to 8.0, the sample was circulated through a preactivated cryogel column at a flow rate of 1 mL/min for 60 min. The unbound bacteria were collected and quantified. The spiked milk sample without treatment with cryogel was used as a control.

Characterization. Attenuated total reflection infrared analysis was performed on a Thermo Fisher Scientific FT-IR instrument (Thermo Fisher Scientific Inc., Waltham, MA, USA). SEM characterization was performed on a JEOL scanning electron microscope (JSM-6700F, JEOL, Japan). Optical absorbance and transmittance analyses were performed on a UV−vis spectrophotometer (NanoPhotometer Pearl, Germany). Gel permeation chromatography (GPC) was carried out at the Institute of Polymer Chemistry, Johannes Kepler University Linz. A Viscothek GPCmax instrument equipped with a PFG column (300 mm × 8 mm; 5 μm particle size) and an RI detector from PSS (Mainz, Germany) were used. DMF containing 10 mM LiBr was used as the mobile phase at a flow rate of 0.75 mL/min at 60 °C. The ^{1}H NMR spectrum was obtained on a Bruker DR X400 spectrometer at 400.13 MHz using DMSO-d_6 as a solvent (δ = 2.5 ppm). Elemental analysis of boron was performed on an Agilent 5110 ICP-OCE (Agilent Technologies). The surface area of cryogels was analyzed by mercury intrusion porosimetry and performed by Micromeritics Instrument Corporation (China).

To investigate the swelling degree (g H_2O/g cryogel), AG and AG-alkyne@polymer-pBA cryogels were first dried at 60 °C in an oven overnight and then weighed. The cryogel was immersed in distilled water for 1 h to ensure complete swelling at ambient temperature. Then, it was put on a filter paper to remove the excess water and weighed. Three replications were made in each case. The swelling degree of the cryogels was determined using the equation[40,41]

$$\text{swelling degree} = \frac{(W_1 - W_2)}{W_2} \quad (2)$$

where W_1 and W_2 are the weight of the swollen and the dry cryogel, respectively.

In the next step, the swollen cryogel was squeezed to remove the water, and the weight of the squeezed cryogel (W_3) was measured again. The macroporosity (%) of the cryogel was determined based on water vapor adsorption and calculated using the equation[41]

$$\text{macroporosity (\%)} = \frac{(W_1 - W_3)/\rho_{H_2O}}{W_1/\rho_{gel}} \quad (3)$$

where ρ_{H_2O} and ρ_{gel} are the density of water at 25 °C and the density of swollen cryogel, respectively.

For SEM analysis, the cryogels containing bacteria were first washed thoroughly with PBS (0.01 M, pH 8.0) to remove the loosely bound bacteria and then fixed with 2.5% glutaraldehyde in PBS (0.01 M, pH 7.4) for 2 h at room temperature. The fixed samples were washed thoroughly with PBS (0.01 M, pH 7.4) and dehydrated by washing with PBS containing an increasing amount of ethanol (20, 40, 60, 80, and 99.5%, v/v) consecutively. The samples were finally immersed in isoamyl acetate at 4 °C overnight and then lyophilized for imaging.

RESULTS AND DISCUSSION

The modular approach to synthesize boronic acid-functionalized cryogels is shown in Scheme 1. The functionalized cryogels were designed to enable bacterial separation based on their macroporous structure and the selective interactions between the boronic acid ligands and bacterial cells. A general-purpose, epoxide-containing cryogel (AG) was first synthesized by cryogelation polymerization. The surface epoxide groups were converted into terminal azide and alkyne groups by reacting AG with sodium azide and alkynyl amine, respectively.

https://dx.doi.org/10.1021/acs.jafc.0c06052
J. Agric. Food Chem. 2021, 69, 135−145

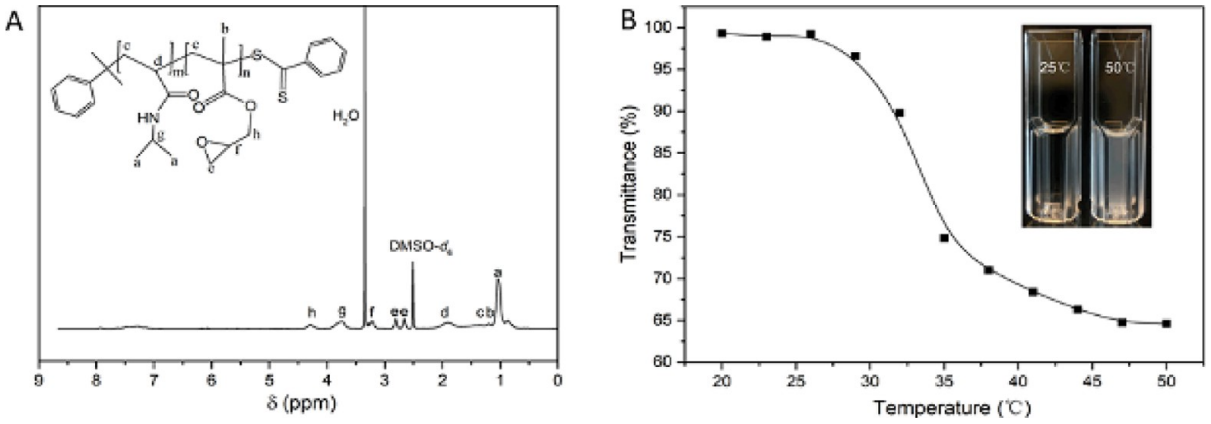

Figure 1. (A) ^{1}H NMR spectrum of poly(NIPAm-*co*-GMA). (B) Temperature-dependent phase transition of poly(NIPAm-*co*-GMA)@N_3 in water (0.4 mg/mL) monitored by measurement of transmittance at 600 nm. The polymer solution was heated at different temperatures for 5 min before its transmittance was measured.

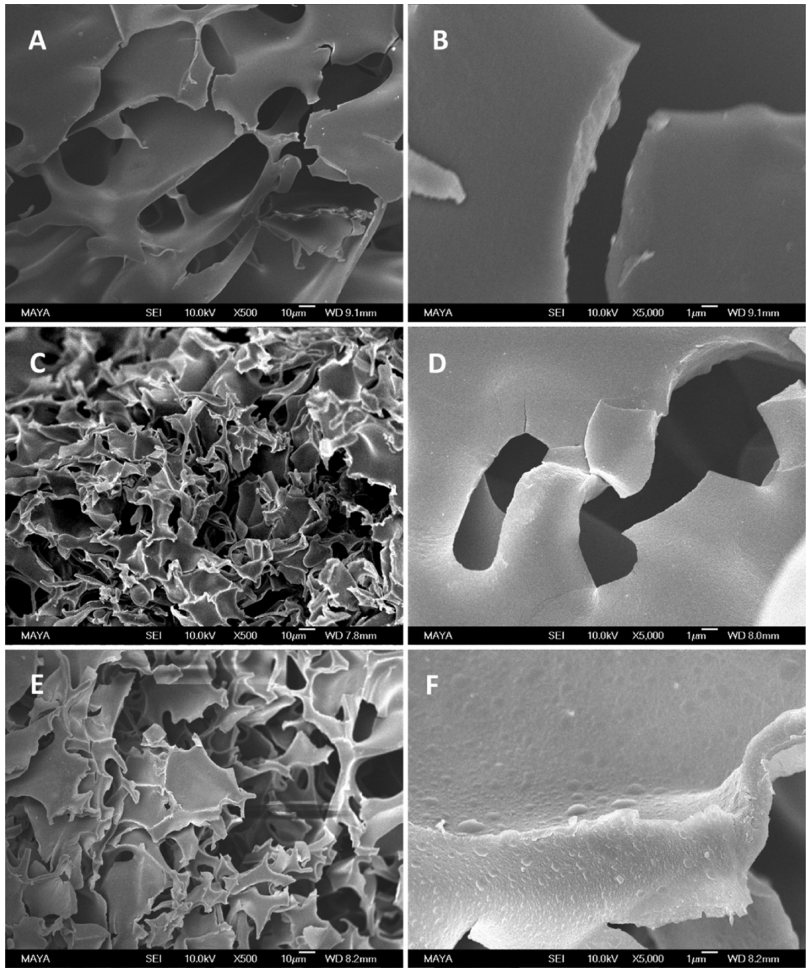

Figure 2. SEM images of AG cryogel (A,B), AG-BA cryogel (C,D), and AG-alkyne@polymer-pBA cryogel (E,F). The scale bars are 10 μm in (A,C,E) and 1 μm in (B,D,F).

The two types of the obtained macroporous cryogels are able to act as a generic support to immobilize a large variety of affinity ligands using the high-efficiency CuAAC and Cu-free click reactions.[42,43] In addition to direct conjugation of the affinity ligand, this work also explores the use of flexible polymer chains to improve the capacity and stimuli-responsive property of macroporous affinity materials.

Synthesis and Characterization of the Polymer. The thermoresponsive copolymer was first synthesized by RAFT polymerization. RAFT polymerization is well-known for its excellent functional group tolerance and general applicability for the synthesis of well-defined and water-soluble polymers.[44] Figure 1A shows the ^{1}H NMR spectrum of the poly(NIPAm-*co*-GMA) used in this work. The ^{1}H NMR spectrum has well-resolved proton signals from the isopropyl group (−CH-

https://dx.doi.org/10.1021/acs.jafc.0c06052
J. Agric. Food Chem. 2021, 69, 135−145

$(CH_3)_2$, 3.73 ppm (g) and 1.04 ppm (a)) of NIPAm,[45] and the CH−$\boldsymbol{CH_2}$−O (2.80 ppm (e) and 2.65 ppm (e)) and $\boldsymbol{CH}$−CH_2−O (3.22 ppm (f)) from GMA. The signal located at 4.28 ppm (h) is assigned to the methylene linked to the ester group in GMA.[46] Based on the ratio of the integrated peak area between NIPAm (a) and GMA (e), the ratio of NIPAm:GMA in the final poly(NIPAm-*co*-GMA) is calculated to be approximately 1.9:1.

The chemical compositions of poly(NIPAm-*co*-GMA) and poly(NIPAm-*co*-GMA)@N_3 were analyzed by FTIR spectroscopy (Figure S1). Absorption bands at 1650 and 1535 cm^{-1} arising from −C═O and −N−H stretching of the amide group can be observed from both spectra. The presence of the epoxy group from the GMA monomer is also confirmed by the characteristic absorption bands at 840 and 910 cm^{-1}. After the introduction of pendent azide groups, the polymer exhibited the characteristic IR band for organic azide at 2100 cm^{-1} (Figures 1 and S1b). The azide-functionalized polymer poly(NIPAm-*co*-GMA)@N_3 has a molecular weight M_n of 21,000 g/mol and molecular weight distribution of 1.9, as determined by GPC analysis (Figure S2).

The introduction of the azide group is accompanied by the addition of the hydroxyl group to the polymer chains, which improves the hydrophilicity of the polymer crucial for capturing bacteria.[21] The incorporated pNIPAm segment in the polymer chain is expected to undergo dehydration and interchain aggregation when the temperature increases above its lower critical solution temperature (LCST). The aggregation of pNIPAm can cause an obvious change in optical transmittance of the polymer solution. As shown in Figure 1B, the transmittance decreased significantly with the increased temperature from 20 to 50 °C. The transmittance dropped abruptly at 32 °C, which is consistent with the LCST of pNIPAm.[28]

Synthesis and Characterization of the Composite Cryogel. The cryogel base AG used in this work was synthesized by copolymerization of Am, MBAm, and AGE in water at −12 °C. The yield of the cryopolymerization was >96%.[32,34] The interior morphologies of the cryogel after different stages of functionalization are shown in Figures 2 and S3. All the cryogels have large interconnected pores with the pore size in the range of 10−80 μm. In comparison with the size of *E. coli* (0.4−0.7 μm by 1−3 μm) and *S. epidermidis* (radius 0.8 μm), the size of the macropores of cryogel is very large, which is advantageous for bacterial binding. These large pores are formed because of the presence of ice crystals during the cryopolymerization.[34,36] The highly porous structure and large interconnected pores endow the cryogel with efficient mass transfer and fast flow through even for particulate-containing samples.[34] In comparison with conventional separation materials such as membranes and filters and so forth, cryogels are of particular interest for bacterial separation because their hydrophilic and soft texture can provide a more cell-compatible environment during the separation. No significant difference was observed after the cryogel base was functionalized with small molecules, for example, after the introduction of azide (Figure S3A), PCAPBA (Figure 2C), and alkynyl group (Figure S3C). The surface of the cryogels remained smooth. On the other hand, after the introduction of the copolymer poly(NIPAm-*co*-GMA)@N_3 to AG-alkyne, a layer of polymer granules can be seen on the interior surface of AG-alkyne@polymer-N_3 (Figure S3E). The roughening of the surface can be explained as a result of immobilization of the thermoresponsive polymer at temperature above its LCST. It should be mentioned that the subsequent introduction of PCAPBA to AG-alkyne@polymer-N_3 did not change the surface morphology of the final material AG-alkyne@polymer-pBA (Figure 2E). Mercury intrusion porosimetry analysis revealed that the total pore area of AG cryogel and AG-alkyne@polymer-pBA is 1.67 and 1.84 m^2/g, while their average pore diameters are determined as 20.8 and 19.2 μm, respectively. Immobilization of the polymer chain caused only slight change in the surface area and pore diameter of the cryogel. The density of AG and AG-alkyne@polymer-pBA was found to be ∼0.05 and ∼0.06 g/mL, respectively. Compared to the base cryogel AG, the mass of the boronic acid-functionalized AG-alkyne@polymer-pBA increased by ∼20%. This polymer density in cryogel is lower than that achieved by surface-initiated polymerization reported in our previous work.[34] Nevertheless, the click conjugation of the azide-functionalized polymer to cryogel is much easier to carry out, which is attractive for practical applications.

The chemical compositions of the composite cryogels were analyzed by FTIR spectroscopy (Figure 3). The presence of

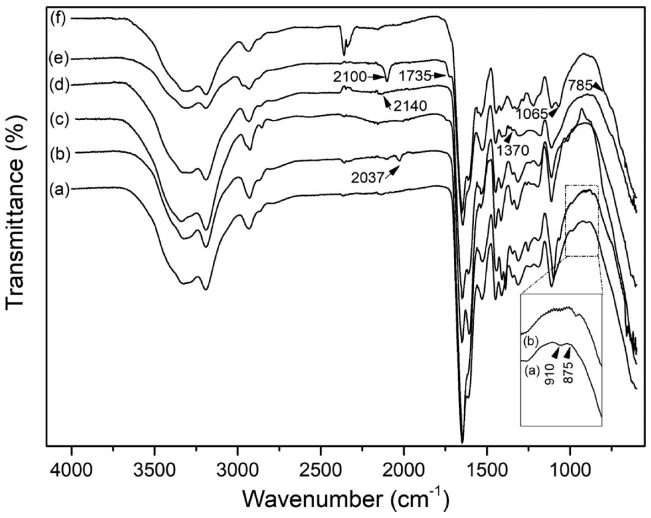

Figure 3. FTIR spectra of (a) AG cryogel, (b) AG-N_3 cryogel, (c) AG-BA cryogel, (d) AG-alkyne cryogel, (e) AG-alkyne@polymer-N_3 cryogel, and (f) AG-alkyne@polymer-pBA cryogel.

two absorption bands at 875 and 910 cm^{-1} indicates the successful incorporation of epoxy groups in cryogel AG (Figure 3a). The changes in the FTIR spectra of the different functionalized cryogels reflect the chemical modifications in the subsequent steps. After introducing azide and alkynyl groups, the epoxy bands disappeared completely, and new absorption bands appeared (Figure 3b,d). The IR bands at 2037 and 2140 cm^{-1} are related to the stretching vibration of azide groups and alkyne groups, respectively. After introducing alkyne-tagged boronic acid on AG-N_3 *via* CuAAC click reaction, the azide absorption band disappeared completely (Figure 3c). Following the conjugation of poly(NIPAm-*co*-GMA)@N_3 to AG-alkyne, the cryogel displayed new absorption bands at 1735 and 1370 cm^{-1}, which were assigned to the ester carbonyl group and the antisymmetric stretching of the carbonyl group, respectively (Figure 3e). Besides, a characteristic azide band at 2100 cm^{-1} appeared because of the remaining azide groups in the polymer after the click conjugation to the cryogel (Figure 3e). After the final

https://dx.doi.org/10.1021/acs.jafc.0c06052
J. Agric. Food Chem. 2021, 69, 135−145

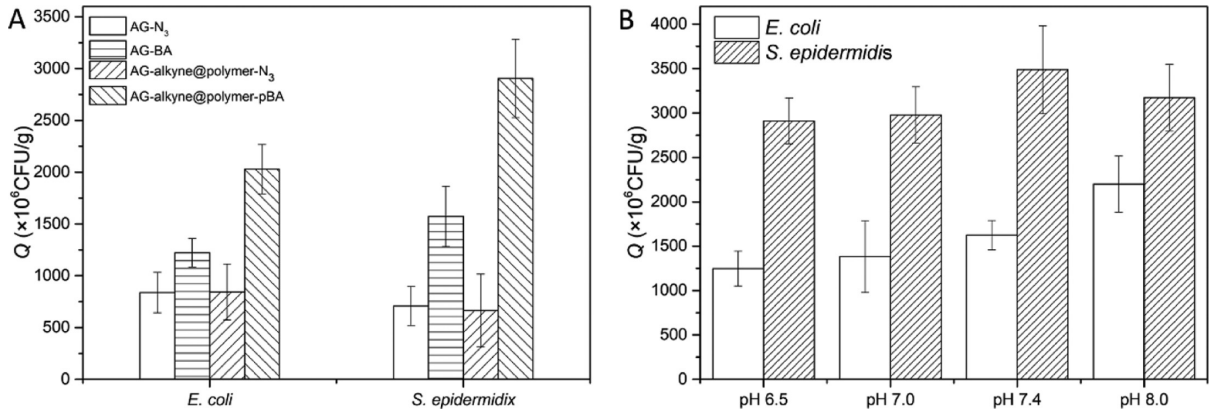

Figure 4. (A) Binding of *E. coli* and *S. epidermidis* by different composite cryogels at pH 8.0. (B) Effect of pH on bacterial binding with AG-alkyne@polymer-pBA. The initial OD_{600} values of the bacterial suspensions were adjusted to ∼1.9 by dilution with 0.01 M PBS.

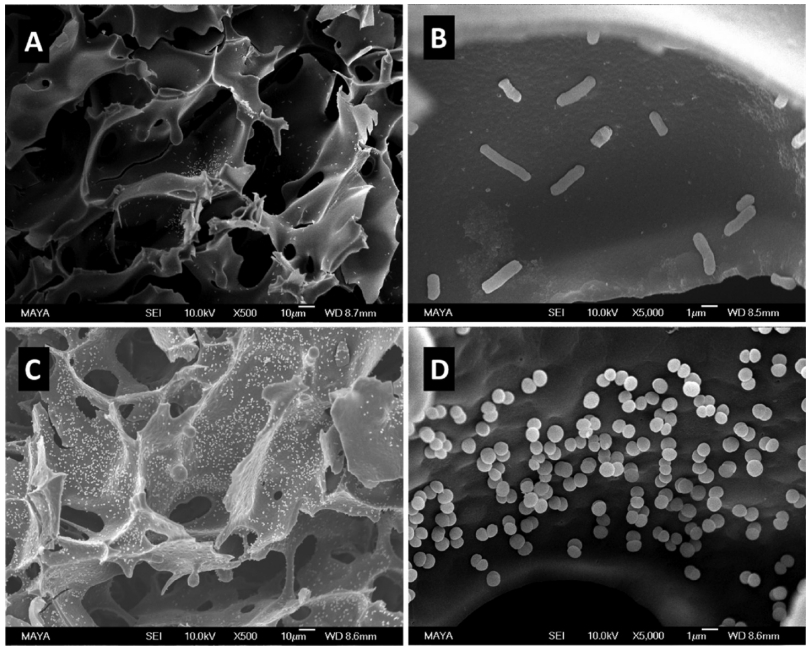

Figure 5. SEM images of AG-alkyne@polymer-pBA cryogel with bound *E. coli* (A,B) and *S. epidermidis* (C,D). The scale bars are 10 μm in (A,C) and 1 μm in (B,D).

introduction of the alkyne-tagged boronic acid, the azide band almost disappeared completely in the spectrum of AG-alkyne@polymer-pBA, suggesting the successful introduction of the boronic acid ligand (Figure 3f). Besides, the characteristic bands at 785 and 1065 cm^{-1} corresponding to the phenyl hydrogen on the boronic acid were also observed (Figure 3f). Elemental analysis revealed that the contents of boron in AG-BA and AG-alkyne@polymer-pBA were 0.033 and 0.618 mg/g, respectively. Based on the boron content, the densities of the boronic acid ligand in AG-BA and AG-alkyne@polymer-pBA are estimated to be 0.0031 and 0.057 mmol/g, respectively.

The swelling degree and macroporosity (volume %) of AG and AG-alkyne@polymer-pBA cryogel are shown in Table S1. The swelling degree of the cryogel decreased after the introduction of the polymer and boronic acid ligands, which can be attributed to the hydrophobic pGMA segment in the polymer. Because of the dehydration and aggregation of the incorporated pNIPAm segment above its LCST, the swelling degree of AG-alkyne@polymer-pBA cryogel decreased further when temperature was increased to 40 °C. The macroporosity also decreased after the introduction of boronic acid-integrated polymer, which is due to the added layer of polymer granules on the interior surface of AG-alkyne@polymer-pBA.

Evaluation of AG-alkyne@polymer-pBA for Bacterial Separation. To evaluate the practicability of AG-alkyne@polymer-pBA for separation of bacteria, *E. coli* and *S. epidermidis* were selected as models to represent Gram-negative and Gram-positive bacteria. For the quantification of bacterial concentration, two calibration plots were established by plotting the optical density (OD_{600}) against the colony-forming unit (cfu) of bacterial suspensions (Figure S4). The affinity of boronate-functionalized materials toward bacteria relies on the formation of cyclic ester between boronic acid and *cis*-diols on the bacterial surface.[21] Apart from boronate affinity interaction, other interactions, including ionic interaction, van der Waals force, and hydrophobic effect, may also affect bacterial binding. Besides, the immobilized polymer chains on the cryogel are expected to provide a flexible interface to improve bacterial binding through polyvalent interactions with the bacteria. To investigate the effect of the

https://dx.doi.org/10.1021/acs.jafc.0c06052
J. Agric. Food Chem. 2021, 69, 135−145

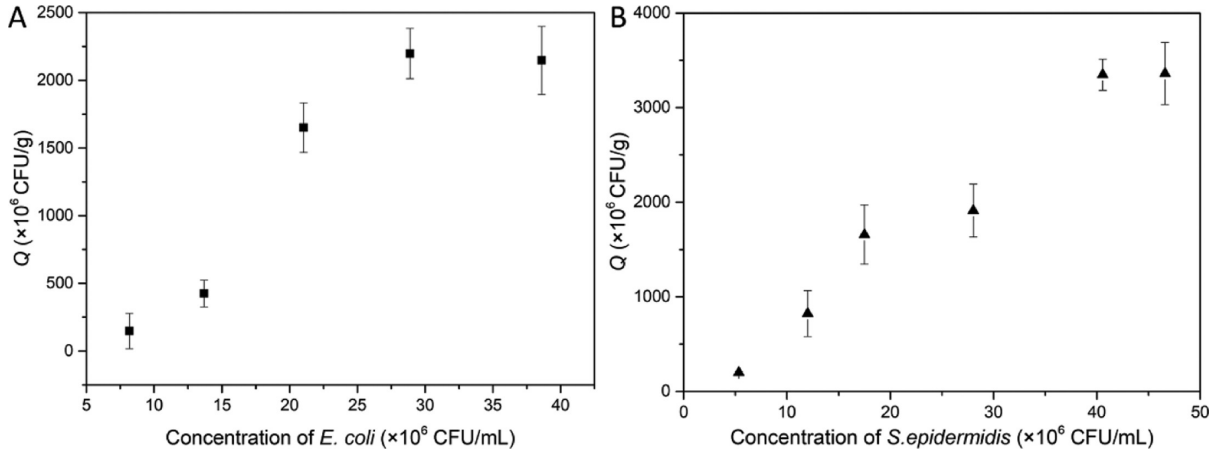

Figure 6. (a) *E. coli* binding isotherm on AG-alkyne@polymer-pBA measured at pH 8.0. (b) *S. epidermidis* binding isotherm on AG-alkyne@polymer-pBA measured at pH 8.0.

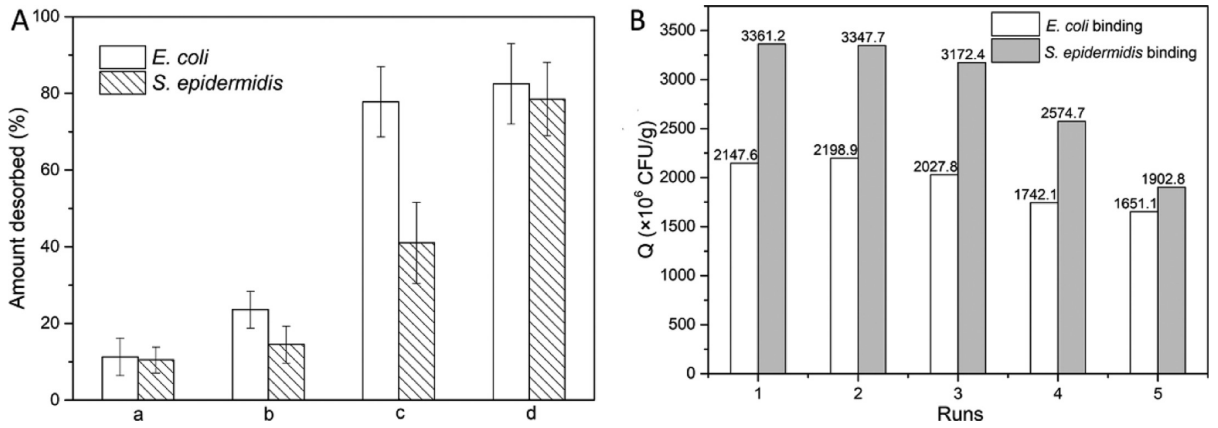

Figure 7. (A) Amount of *E. coli* and *S. epidermidis* desorbed from AG-alkyne@polymer-pBA cryogel in different elution media: (a) 0.2 M acetate buffer (pH 4.0, containing 0.5 M NaCl), (b) 0.1 M fructose in PBS (20 mM, pH 9.0, containing 0.5 M NaCl), (c) 0.2 M fructose in PBS (20 mM, pH 9.0, containing 0.5 M NaCl), and (d) 0.5 M fructose in PBS (20 mM, pH 9.0, containing 0.5 M NaCl). (B) Recycle and reuse of AG-alkyne@polymer-pBA cryogel for affinity separation of *E. coli* and *S. epidermidis*.

immobilized boronic acid on bacterial binding, the cryogels after different functionalization stages were tested to measure their capability to bind *E. coli* and *S. epidermidis*. As shown in Figure 4A, AG-BA and AG-alkyne@polymer-pBA cryogel exhibited significantly higher binding toward the two model bacteria than AG-N_3 and AG-alkyne@polymer-N_3, indicating that the boronic acid plays a crucial role in bacterial binding. Compared to AG-BA that contains boronic acid directly fixed on the surface, AG-alkyne@polymer-pBA exhibited much higher bacterial binding. The enhanced bacterial binding can be attributed to the flexible intermediate polymer chains, through which more boronic acid ligands are immobilized in AG-alkyne@polymer-pBA.

Normally, boronate affinity separation needs to be performed at high pH (pH > 8.0) to ensure covalent binding. The high pH condition is not suitable for alkaline-labile biomolecules. As multiple boronic acid ligands are presented in the polymer-containing cryogel AG-alkyne@polymer-pBA, we expected that effective bacterial binding could be achieved at close to neutral pH. Figure 4B shows the effect of pH on bacterial binding in the range of pH 6.5−8.0. For *S. epidermidis*, the bacterial binding was insensitive to variation of pH in the range of 6.5−8.0, while the binding of *E. coli* increased gradually when the pH was changed from 6.5 to 8.0.

From the SEM images in Figure 5, it is clear that the bacterial cells bound in the cryogel are evenly distributed on the interior surface, and no significant disintegration of bacterial cells was observed. The density of bound *S. epidermidis* on the surface of AG-alkyne@polymer-pBA is higher than that of *E. coli*, which is in accordance with the binding results measured with the two model bacteria (Figure 4B).

The equilibrium binding isotherms of AG-alkyne@polymer-pBA for the two model bacteria are shown in Figure 6. The binding capacities of the cryogel toward *E. coli* and *S. epidermidis* are 2.15×10^9 and 3.36×10^9 cfu/g, respectively. In terms of binding capacity, the composite cryogel does not appear better than some previous nanoparticle-based separation materials (Table S2). Nevertheless, the large pores in the cryogel make it possible to separate bacteria in the chromatography mode more conveniently, and the cryogel can be easily regenerated for repeated use. Compared with AG-BA, the higher binding capacities of AG-alkyne@polymer-pBA are mainly attributed to the multiple boronic acid ligands immobilized through the polymer chains in the cryogel.

The reusability of the AG-alkyne@polymer-pBA cryogel is essential from the view point of both research and industry. Therefore, the elution of bacterial cells and the reuse of AG-alkyne@polymer-pBA cryogel for the separation of *E. coli* and

https://dx.doi.org/10.1021/acs.jafc.0c06052
J. Agric. Food Chem. 2021, 69, 135−145

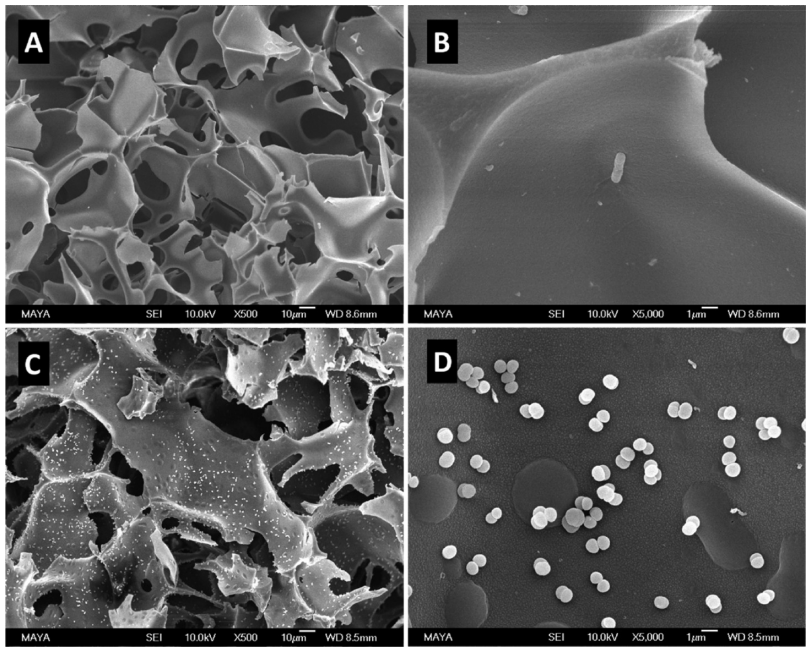

Figure 8. SEM images of AG-alkyne@polymer-pBA cryogel loaded with *E. coli* (A,B) and *S. epidermidis* (C,D). The images were taken after the bacteria were eluted using 0.2 M fructose (pH 9.0, 20 mM, PBS, containing 0.5 M NaCl). The scale bars are 10 μm in (A,C) and 1 μm in (B,D).

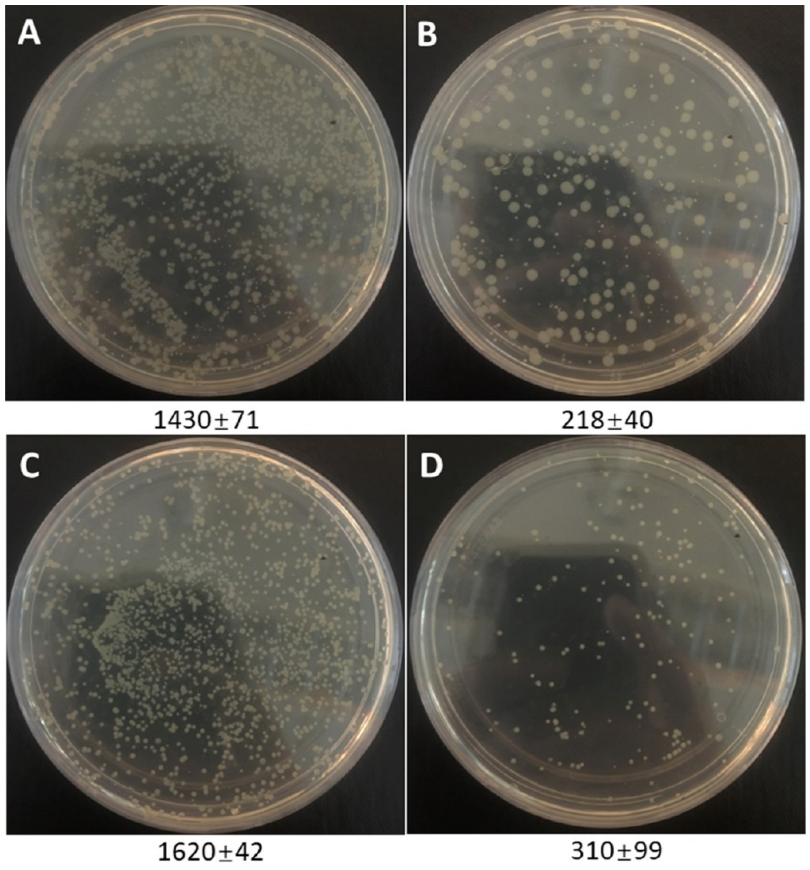

Figure 9. Separation of *E. coli* and *S. epidermidis* from the spiked 25% milk sample using AG-alkyne@polymer-pBA. (A) *E. coli* in the spiked milk; (B) remaining *E. coli* in the spiked milk after treatment with the cryogel; (C) *S. epidermidis* in the spiked milk; and (D) remaining *S. epidermidis* in the spiked milk after treatment with the cryogel.

S. epidermidis were also investigated. The possibility of using the thermoresponsive phase transition of the polymer to desorb the bound bacteria was studied first. Unfortunately, in the binding buffer, the desorption of the bound bacteria was less than 10% when the temperature was increased to 37 °C (date not shown). The inefficient thermoelution may be

https://dx.doi.org/10.1021/acs.jafc.0c06052
J. Agric. Food Chem. 2021, 69, 135−145

explained by the slow phase transition of the polymer chains,[47] especially when the polymer was conjugated to the cryogel surface through multiple covalent triazole linkers. Figure 7A shows the results of bacterial desorption from AG-alkyne@polymer-pBA in different elution media. Because of the multiple boronate ester bonds, the binding between the boronic acid-functionalized cryogel and the bacterial cell is too strong to be disrupted by the acidic buffer (pH 4.0). To avoid disintegration of bacterial cells in strong acidic media, a different elution strategy using fructose was tested. As shown in Figure 7A, around 70% of the loaded *E. coli* and *S. epidermidis* can be eluted by 0.2 and 0.5 M fructose−PBS solution, respectively. The result indicates the higher binding strength of AG-alkyne@polymer-pBA to *S. epidermidis* than *E. coli* probably because of the difference in the saccharide structure on the different bacterial surfaces. SEM analysis also indicates the efficiency of 0.2 and 0.5 M fructose−PBS solution to elute *E. coli* and *S. epidermidis* from AG-alkyne@polymer-pBA cryogel (Figures 8 and S5). After being eluted with 0.2 and 0.5 M fructose−PBS solution, the cryogel was washed with 0.01 M PBS (pH 8.0) followed by fixing with glutaraldehyde, dehydrating by PBS−ethanol solution, and lyophilizing for imaging. As shown in Figures 8 and S5, the small number of remaining bacteria on the composite cryogel indicates the efficiency of 0.2 and 0.5 M fructose−PBS solution to elute *E. coli* and *S. epidermidis*. After the eluted bacteria were transferred into LB medium and cultivated for 16 h, the cell density increased significantly, indicating the presence of viable bacteria in the eluted fraction (Figure S6).

The binding and elution of *E. coli* and *S. epidermidis* with AG-alkyne@polymer-pBA cryogel were also studied in a chromatography mode (Figure S7). From the chromatography results, it is clear that the two model bacteria can be recovered using 0.5 M fructose−PBS effectively. The large peak from the acetic acid washing was mainly due to the change in optical transmittance when the mobile phase was switched to the acidic washing. In a control experiment, a column packed with AG-BA was also examined. The elution peaks for the two bacteria from AG-BA are smaller than from AG-alkyne@polymer-pBA, indicating that the polymer-containing cryogel provides better bacterial separation in the chromatography mode.

The reusability of AG-alkyne@polymer-pBA cryogel for the separation of *E. coli* and *S. epidermidis* was also investigated. After eluting the bound *E. coli* and *S. epidermidis* with 0.5 M fructose−PBS buffer, the cryogel was washed with 100 mM acetic acid and water to remove the bound fructose and the residual bacterial cells. The cryogel was reactivated by loading PBS buffer (0.01 M, pH 8.0) before the next binding experiment was performed. As shown in Figure 7B, in the first three runs of bacterial separation, the binding capacities of the cryogel kept almost unchanged. After three runs of separation, the binding capacities decreased to around 80% of the original value. The reduction of binding capacity may be attributed to the loss of some of the boronic acid ligands or incomplete removal of the microbial cells from the previous circle.

Separation of Bacteria from Complex Samples. To investigate the applicability of AG-alkyne@polymer-pBA to separate bacteria in complex samples, the bacterial separation was tested with a diluted milk sample (4× diluted) spiked with *E. coli* and *S. epidermidis* (at ~10^3 cell/mL). After adjusting the pH to 8.0, the samples were circulated through the cryogel column at a flow rate of 1 mL/min for 60 min. The number of unbound bacteria was quantified by the conventional viable counting method. As shown in Figure 9, most of the bacterial cells were captured by the cryogel. Considering the abundance of interfering substances in milk such as proteins, lipids, carbohydrates, and so forth, the cryogel exhibited high effectiveness for the removal of bacteria.

In summary, a novel boronic acid-functionalized, macroporous cryogel was prepared for the selective separation of bacteria. The method of material synthesis is based on a versatile polymer building block and high-efficiency click chemistry. The RAFT polymerization provides a facile and versatile means to synthesize a well-controlled polymer with specific structural and functional moieties, and the CuAAC click chemistry enables straightforward assembly of the functionalized cryogels. Using an intermediate polymer layer, the number of immobilized boronic acid ligands in the cryogel is increased, leading to a higher bacterial-binding capacity. In comparison with other cryogels reported in the literature, the boronic acid-modified cryogel described in this work has simpler synthesis procedure and higher ligand density (Table S3). Owing to the high density of affinity ligands appended on the flexible polymer chains, the new composite cryogel exhibited excellent affinity toward both Gram-positive and Gram-negative bacteria. Most importantly, the macroporous structure of cryogel makes it possible to realize direct separation and isolation of bacteria from complex media. The synthetic methods developed in this work will be of generic use for constructing polymer-based affinity materials for the separation of large biomolecules and biomolecular assemblies, including viruses and cells.

■ ASSOCIATED CONTENT

Supporting Information

The Supporting Information is available free of charge at https://pubs.acs.org/doi/10.1021/acs.jafc.0c06052.

FTIR spectra of poly(NIPAm-*co*-GMA) and poly(NIPAm-*co*-GMA)@N_3; GPC trace of poly(NIPAm-*co*-GMA)@N_3; SEM images of cryogels AG-N_3, AG-alkyne, and AG-alkyne@polymer-N_3; calibration plots for quantification of *E. coli* and *S. Epidermidis*; SEM images of AG-alkyne@polymer-pBA cryogel containing uneluted *S. Epidermidis*; cultivation of bacteria *E. coli* and *S. epidermidis* cells eluted from cryogel; capture and elution of bacteria in cryogel column; swelling degree and macroporosity of cryogels; comparison of binding capacities of different adsorbents toward bacteria; and comparison of different composite cryogels for chromatographic separation (PDF)

■ AUTHOR INFORMATION

Corresponding Author

Lei Ye − *Division of Pure and Applied Biochemistry, Department of Chemistry, Lund University, 221 00 Lund, Sweden;* orcid.org/0000-0002-3646-4072; Email: lei.ye@tbiokem.lth.se

Authors

Hongwei Zheng − *Division of Pure and Applied Biochemistry, Department of Chemistry, Lund University, 221 00 Lund, Sweden; Food Safety Laboratory, College of Food Science &*

https://dx.doi.org/10.1021/acs.jafc.0c06052
J. Agric. Food Chem. 2021, 69, 135−145

Engineering, Ocean University of China, Qingdao 266003, China

Solmaz Hajizadeh − *Division of Pure and Applied Biochemistry, Department of Chemistry, Lund University, 221 00 Lund, Sweden;* orcid.org/0000-0002-0348-8756

Haiyue Gong − *Division of Pure and Applied Biochemistry, Department of Chemistry, Lund University, 221 00 Lund, Sweden*

Hong Lin − *Food Safety Laboratory, College of Food Science & Engineering, Ocean University of China, Qingdao 266003, China*

Complete contact information is available at: https://pubs.acs.org/10.1021/acs.jafc.0c06052

Notes

The authors declare no competing financial interest.

■ ACKNOWLEDGMENTS

This work was supported by the Swedish Research Council VR (grant number 2019-04228). H.Z. thanks the China Scholarship Council (CSC) for a visiting scholarship. H.Z. is a visiting Ph.D. student in Lund University and a Ph.D. candidate in Ocean University of China.

■ REFERENCES

(1) Jayan, H.; Pu, H.; Sun, D.-W. Recent development in rapid detection techniques for microorganism activities in food matrices using bio-recognition: A review. *Trends Food Sci. Technol.* **2020**, *95*, 233−246.

(2) Long, S.; Miao, L.; Li, R.; Deng, F.; Qiao, Q.; Liu, X.; Yan, A.; Xu, Z. Rapid Identification of Bacteria by Membrane-Responsive Aggregation of a Pyrene Derivative. *ACS Sens.* **2019**, *4*, 281−285.

(3) Ho, C.-S.; Jean, N.; Hogan, C. A.; Blackmon, L.; Jeffrey, S. S.; Holodniy, M.; Banaei, N.; Saleh, A. A. E.; Ermon, S.; Dionne, J. Rapid identification of pathogenic bacteria using Raman spectroscopy and deep learning. *Nat. Commun.* **2019**, *10*, 4927.

(4) Batt, C. A. Materials science. food pathogen detection. *Science* **2007**, *316*, 1579−1580.

(5) Liu, Y.; Zhou, H.; Hu, Z.; Yu, G.; Yang, D.; Zhao, J. Label and label-free based surface-enhanced Raman scattering for pathogen bacteria detection: A review. *Biosens. Bioelectron.* **2017**, *94*, 131−140.

(6) Kant, K.; Shahbazi, M.-A.; Dave, V. P.; Ngo, T. A.; Chidambara, V. A.; Than, L. Q.; Bang, D. D.; Wolff, A. Microfluidic devices for sample preparation and rapid detection of foodborne pathogens. *Biotechnol. Adv.* **2018**, *36*, 1003−1024.

(7) Stevens, K. A.; Jaykus, L.-A. Bacterial separation and concentration from complex sample matrices: a review. *Crit. Rev. Microbiol.* **2004**, *30*, 7−24.

(8) Majdinasab, M.; Hayat, A.; Marty, J. L. Aptamer-based assays and aptasensors for detection of pathogenic bacteria in food samples. *TrAC, Trends Anal. Chem.* **2018**, *107*, 60−77.

(9) Dong, Q.; Chi, S.-S.; Deng, X.-Y.; Lan, Y.-H.; Peng, C.; Dong, L.-Y.; Wang, X.-H. Boronate affinity monolith via two-step atom transfer radical polymerization for specific capture of cis-diol-containing compounds. *Eur. Polym. J.* **2018**, *100*, 270−277.

(10) Jin, S.; Zhang, W.; Yang, Q.; Dai, L.; Zhou, P. An inorganic boronate affinity in-needle monolithic device for specific capture of cis-diol containing compounds. *Talanta* **2018**, *178*, 710−715.

(11) Zheng, H.; Lin, H.; Chen, X.; Tian, J.; Pavase, T. R.; Wang, R.; Sui, J.; Cao, L. Development of Boronate Affinity-based Magnetic Composites in Biological Analysis: Advances and Future Prospects. *TrAC, Trends Anal. Chem.* **2020**, *129*, 115952.

(12) Li, D.; Tu, T.; Wu, X. Efficient preparation of template immobilization-based boronate affinity surface-imprinted silica nanoparticles using poly(4-aminobenzyl alcohol) as an imprinting coating for glycoprotein recognition. *Anal. Methods* **2018**, *10*, 4419−4429.

(13) Li, D.; Bie, Z.; Wang, F.; Guo, E. Efficient synthesis of riboflavin-imprinted magnetic nanoparticles by boronate affinity-based surface imprinting for the selective recognition of riboflavin. *Analyst* **2018**, *143*, 4936−4943.

(14) Tang, S.; Ma, H.; Tu, H.-C.; Wang, H.-R.; Lin, P.-C.; Anseth, K. S. Adaptable Fast Relaxing Boronate-Based Hydrogels for Probing Cell−Matrix Interactions. *Adv. Sci.* **2018**, *5*, 1800638.

(15) Zhao, S.; Zou, Y.; Wang, Y.; Zhang, H.; Liu, X. Organized cryogel composites with 3D hierarchical porosity as an extraction adsorbent for nucleosides. *J. Sep. Sci.* **2019**, *42*, 2140−2147.

(16) Li, D.; Wang, N.; Wang, F.; Zhao, Q. Boronate affinity-based surface-imprinted quantum dots as novel fluorescent nanosensors for the rapid and efficient detection of rutin. *Anal. Methods* **2019**, *11*, 3212−3220.

(17) Sun, X.; Chapin, B. M.; Metola, P.; Collins, B.; Wang, B.; James, T. D.; Anslyn, E. V. The mechanisms of boronate ester formation and fluorescent turn-on in ortho-aminomethylphenylboronic acids. *Nat. Chem.* **2019**, *11*, 768−778.

(18) Bie, Z.; Zhao, W.; Lv, Z.; Liu, S.; Chen, Y. Preparation of Salbutamol imprinted magnetic nanoparticles via boronate affinity oriented surface imprinting for selective analysis of trace salbutamol residues. *Analyst* **2019**, *144*, 3128−3135.

(19) Liu, Z.; He, H. Synthesis and applications of boronate affinity materials: from class selectivity to biomimetic specificity. *Acc. Chem. Res.* **2017**, *50*, 2185−2193.

(20) Li, D.; Tu, T.; Yang, M.; Xu, C. Efficient preparation of surface imprinted magnetic nanoparticles using poly (2-anilinoethanol) as imprinting coating for the selective recognition of glycoprotein. *Talanta* **2018**, *184*, 316−324.

(21) Zheng, H.; Han, F.; Lin, H.; Cao, L.; Pavase, T. R.; Sui, J. Preparation of a novel polyethyleneimine functionalized sepharose-boronate affinity material and its application in selective enrichment of food borne pathogenic bacteria. *Food Chem.* **2019**, *294*, 468−476.

(22) Golabi, M.; Kuralay, F.; Jager, E. W. H.; Beni, V.; Turner, A. P. F. Electrochemical bacterial detection using poly (3-aminophenylboronic acid)-based imprinted polymer. *Biosens. Bioelectron.* **2017**, *93*, 87−93.

(23) Dechtrirat, D.; Gajovic-Eichelmann, N.; Wojcik, F.; Hartmann, L.; Bier, F. F.; Scheller, F. W. Electrochemical displacement sensor based on ferrocene boronic acid tracer and immobilized glycan for saccharide binding proteins and E. coli. *Biosens. Bioelectron.* **2014**, *58*, 1−8.

(24) Wang, J.; Gao, J.; Liu, D.; Han, D.; Wang, Z. Phenylboronic acid functionalized gold nanoparticles for highly sensitive detection of Staphylococcus aureus. *Nanoscale* **2012**, *4*, 451−454.

(25) Liang, X.; Bonizzoni, M. Boronic acid-modified poly (amido-amine) dendrimers as sugar-sensing materials in water. *J. Mater. Chem. B* **2016**, *4*, 3094−3103.

(26) Zhao, N.; Liu, Z.; Xing, J.; Zheng, Z.; Song, F.; Liu, S. Teamed boronate affinity-functionalized branched polyethyleneimine-modified magnetic nanoparticles for the selective capture of ginsenosides from rat plasma. *Chem. Eng. J.* **2020**, *383*, 123079.

(27) Li, H.; Zhang, X.; Zhang, L.; Cheng, W.; Kong, F.; Fan, D.; Li, L.; Wang, W. Silica stationary phase functionalized by 4-carboxybenzoboroxole with enhanced boronate affinity nature for selective capture and separation of cis-diol compounds. *Anal. Chim. Acta* **2017**, *985*, 91−100.

(28) Zhang, X.; Wang, J.; He, X.; Chen, L.; Zhang, Y. Tailor-Made Boronic Acid Functionalized Magnetic Nanoparticles with a Tunable Polymer Shell-Assisted for the Selective Enrichment of Glycoproteins/Glycopeptides. *ACS Appl. Mater. Interfaces* **2015**, *7*, 24576−24584.

(29) Jiang, L.; Bagán, H.; Kamra, T.; Zhou, T.; Ye, L. Nanohybrid polymer brushes on silica for bioseparation. *J. Mater. Chem. B* **2016**, *4*, 3247−3256.

(30) Su, J.; He, X.; Chen, L.; Zhang, Y. A combination of "thiolene" click chemistry and surface initiated atom transfer radical polymerization: Fabrication of boronic acid functionalized magnetic graphene

oxide composite for enrichment of glycoproteins. *Talanta* **2018**, *180*, 54−60.
(31) Köse, K.; Erol, K.; ÿzgür, E.; Uzun, L.; Denizli, A. PolyAdenine cryogels for fast and effective RNA purification. *Colloids Surf., B* **2016**, *146*, 678−686.
(32) Farías, T.; Hajizadeh, S.; Ye, L. Cryogels with high cisplatin adsorption capacity: Towards removal of cytotoxic drugs from wastewater. *Sep. Purif. Technol.* **2020**, *235*, 116203.
(33) Hajizadeh, S.; Kettisen, K.; Gram, M.; Bülow, L.; Ye, L. Composite imprinted macroporous hydrogels for haemoglobin purification from cell homogenate. *J. Chromatogr. A* **2018**, *1534*, 22−31.
(34) Hajizadeh, S.; Ye, L. Hierarchical macroporous material with dual responsive copolymer brushes and phenylboronic acid ligands for bioseparation of proteins and living cells. *Sep. Purif. Technol.* **2019**, *224*, 95−105.
(35) Srivastava, A.; Shakya, A. K.; Kumar, A. Boronate affinity chromatography of cells and biomacromolecules using cryogel matrices. *Enzyme Microb. Technol.* **2012**, *51*, 373−381.
(36) Kumar, A.; Srivastava, A. Cell separation using cryogel-based affinity chromatography. *Nat. Protoc.* **2010**, *5*, 1737−1747.
(37) Hajizadeh, S.; Kirsebom, H.; Mattiasson, B. Characterization of macroporous carbon-cryostructured particle gel, an adsorbent for small organic molecules. *Soft Matter* **2010**, *6*, 5562−5569.
(38) Hajizadeh, S.; Mattiasson, B.; Kirsebom, H. Flow-Through-Mediated Surface Immobilization of Sub-Micrometre Particles in Monolithic Cryogels. *Macromol. Mater. Eng.* **2014**, *299*, 631−638.
(39) Suksrichavalit, T.; Yoshimatsu, K.; Prachayasittikul, V.; Bülow, L.; Ye, L. "Clickable" affinity ligands for effective separation of glycoproteins. *J. Chromatogr. A* **2010**, *1217*, 3635−3641.
(40) Farías, T.; Hajizadeh, S.; Ye, L. Cryogels with high cisplatin adsorption capacity: Towards removal of cytotoxic drugs from wastewater. *Sep. Purif. Technol.* **2020**, *235*, 116203.
(41) Bakhshpour, M.; Topcu, A. A.; Bereli, N.; Alkan, H.; Denizli, A. Poly(Hydroxyethyl Methacrylate) Immunoaffinity Cryogel Column for the Purification of Human Immunoglobulin. *Mol. Gels* **2020**, *6*, 4.
(42) Bi, C.; Zhao, Y.; Shen, L.; Zhang, K.; He, X.; Chen, L.; Zhang, Y. Click Synthesis of Hydrophilic Maltose-Functionalized Iron Oxide Magnetic Nanoparticles Based on Dopamine Anchors for Highly Selective Enrichment of Glycopeptides. *ACS Appl. Mater. Interfaces* **2015**, *7*, 24670−24678.
(43) Zhang, X.; He, X.; Chen, L.; Zhang, Y. Boronic acid modified magnetic nanoparticles for enrichment of glycoproteins via azide and alkyne click chemistry. *J. Mater. Chem.* **2012**, *22*, 16520−16526.
(44) Chen, X.; Liu, X.; Miao, C.; Song, P.; Xiong, Y. Ionic liquid-like inimer mediated RAFT polymerization of N-isopropylacrylamide. *Eur. Polym. J.* **2018**, *107*, 229−235.
(45) Li, J.-J.; Zhou, Y.-N.; Luo, Z.-H.; Zhu, S. A polyelectrolyte-containing copolymer with a gas-switchable lower critical solution temperature-type phase transition. *Polym. Chem.* **2019**, *10*, 260−266.
(46) Li, P.; Xu, R.; Wang, W.; Li, X.; Xu, Z.; Yeung, K. W. K.; Chu, P. K. Thermosensitive poly (N-isopropylacrylamide-co-glycidyl methacrylate) microgels for controlled drug release. *Colloids Surf., B* **2013**, *101*, 251−255.
(47) Srivastava, A.; Shakya, A. K.; Kumar, A. Boronate affinity chromatography of cells and biomacromolecules using cryogel matrices. *Enzyme Microb. Technol.* **2012**, *51*, 373−381.

https://dx.doi.org/10.1021/acs.jafc.0c06052
J. Agric. Food Chem. 2021, 69, 135−145